frontiers

Author's Proof

Carefully read the entire proof and mark all corrections in the appropriate place, using the Adobe Reader commenting tools (**Adobe Help**). We do not accept corrections in the form of edited manuscripts.

In order to ensure the timely publication of your article, please submit the corrections within 48 hours.
If you have any questions, contact engineering.production.office@frontiersin.org.

Quick Check-List

- **Author names** - Complete, accurate and consistent with your previous publications.
- **Affiliations** - Complete and accurate. Follow this style when applicable: Department, Institute, University, City, Country.
- **Tables** - Make sure our formatting style did not change the meaning/alignment of your Tables.
- **Figures** - Make sure we are using the latest versions.
- **Funding and Acknowledgments** - List all relevant funders and acknowledgments.
- **Conflict of Interest** - Ensure any relevant conflicts are declared.
- **Supplementary files** - Ensure the latest files are published and that no line numbers and tracked changes are visible. Also, the supplementary files should be cited in the article body text.
- **Queries** - Reply to all typesetters queries below.
- **Content** - Read all content carefully and ensure any necessary corrections are made.

Author Queries Form

Query No.	Details Required	Author's Response
Q1	The citation and surnames of all of the authors have been highlighted. Please check all of the names carefully and indicate if any are incorrect. Please note that this may affect the indexing of your article in repositories such as PubMed.	
Q2	Confirm that the email address in your correspondence section is accurate.	
Q3	Please ask the following authors to register with Frontiers (at https://www.frontiersin.org/Registration/Register.aspx) if they would like their names on the article abstract page and PDF to be linked to a Frontiers profile. Please ensure to provide us with the profile link(s) when submitting the proof corrections. Non-registered authors will have the default profile image displayed. "Alistair Rice" "Mariel Gonzalez" "Karla E. Inostroza-Brito." "Estelle Collin.	

Query No.	Details Required	Author's Response
Q4	If you decide to use previously published, copyrighted figures in your article, please keep in mind that it is your responsibility, as the author, to obtain the appropriate permissions and licenses and to follow any citation instructions requested by third-party rights holders. If obtaining the reproduction rights involves the payment of a fee, these charges are to be paid by the authors.	
Q5	Ensure that all the figures, tables and captions are correct, and that all figures are of the highest quality/resolution.	
Q6	Verify that all the equations and special characters are displayed correctly.	
Q7	Ensure to add all grant numbers and funding information, as after publication this is no longer possible.	
Q8	Ensure, if it applies to your study, the ethics statement is included in the article.	
Q9	Please provide the name of the department for the following affiliations. "William Harvey Research Institute, Queen Mary University of London, London, United Kingdom" "Institute of Bioengineering, Queen Mary University of London, London, United Kingdom" "Biodiscovery Institute, University of Nottingham, Nottingham, United Kingdom."	
Q10	Could you please confirm if all author affiliations are fine as listed?	
Q11	Please reduce short running title to maximum of five words.	
Q12	Please provide a minimum of five or maximum of eight keywords.	
Q13	Please provide the "Supplementary Material" as a separate file. This file will be published directly on the online article page, and will not be typeset in the PDF.	
Q14	Please confirm that the Data Availability statement is accurate.	
Q15	Kindly confirm if the details appearing in the "Author Contributions" section are correct and make sure all authors listed in the Author's list are mentioned there.	
Q16	Please provide a revised Author Contribution section including all the authors in the list.	
Q17	The initials "AM" and "AM" used in Author Contribution section is same for the authors "Anna Majkowska" and "Alvaro Mata". Please confirm if "AM" corresponds to "Anna Majkowska" or "Alvaro Mata" in lines 1225.	
Q18	Please provide the city name and publisher name for "Azevedo, 2019."	

Query No.	Details Required	Author's Response
Q19	Please specify the "＊＊＊" inside the artwork of "Figures 2, 5" which is explained in the caption.	
Q20	We have changed "Figures 3F to 3E, 3G to 3F, 3H to 3G" in the captions, text citations, and artwork. Please confirm if this is fine.	
Q21	Please cite "Figure 4A" inside the text.	
Q22	Please cite "Figure 7G" inside the text.	
Q23	Please specify the "＊,＊＊" inside the artwork of "Figure 7" which is explained in the caption.	
Q24	The section "Materials and Methods" is coming after the "Conclusion" section. Please confirm if this is fine.	
Q25	Please confirm whether the insertion of the "Acknowledgments" section is fine.	

frontiers in Materials

ORIGINAL RESEARCH
published: xx May 2020
doi: 10.3389/fmats.2020.00167

Interfacial Self-Assembly to Spatially Organize Graphene Oxide Into Hierarchical and Bioactive Structures

*Anna Majkowska[1,2,3], Carlos Redondo-Gómez[2,3], Alistair Rice[4], Mariel Gonzalez[3], Karla E. Inostroza-Brito[3], Estelle Collin[3], Jose Carlos Rodriguez-Cabello[5], Armando E. Del Rio Hernandez[4], Egle Solito[1] and Alvaro Mata[2,3,6,7,8]**

[1] William Harvey Research Institute, Queen Mary University of London, London, United Kingdom, [2] Institute of Bioengineering, Queen Mary University of London, London, United Kingdom, [3] School of Engineering and Materials Science, Queen Mary University of London, London, United Kingdom, [4] Department of Bioengineering, Imperial College London, London, United Kingdom, [5] BIOFORGE Group, University of Valladolid, CIBER-BBN, Valladolid, Spain, [6] School of Pharmacy, University of Nottingham, Nottingham, United Kingdom, [7] Biodiscovery Institute, University of Nottingham, Nottingham, United Kingdom, [8] Department of Chemical and Environmental Engineering, University of Nottingham, Nottingham, United Kingdom

Multicomponent self-assembly holds great promise for the generation of complex and functional biomaterials with hierarchical microstructure. Here, we describe the use of supramolecular co-assembly between an elastin-like recombinamer (ELR5) and a peptide amphiphile (PA) to organize graphene oxide (GO) flakes into bioactive structures across multiple scales. The process takes advantage of a reaction—diffusion mechanism to enable the incorporation and spatial organization of GO within multiple ELR5/PA layers. Scanning electron microscopy (SEM), transmission electron microscopy (TEM), and ImageJ software were used to demonstrate the hierarchical organization of GO flakes within the ELR5/PA layers and the distribution profiles of GO throughout the ELR5/PA membranes. Furthermore, atomic force microscopy (AFM) revealed improved Young's moduli of the ELR5/PA/GO membranes compared to the ELR5/PA membranes. Lastly, we investigated biocompatibility of the ELR5/PA/GO membrane via various cell culture methods.

Keywords: graphene oxide, multicomponent self-assembly, peptide amphiphiles, elastin-like recombinamer

OPEN ACCESS

Edited by:
Lorenzo Moroni,
Maastricht University, Netherlands

Reviewed by:
John B. Matson,
Virginia Tech, United States
Marcel Bouvet,
Université de Bourgogne, France

***Correspondence:**
Alvaro Mata
a.mata@nottingham.ac.uk

Specialty section:
This article was submitted to Biomaterials, a section of the journal Frontiers in Materials

Received: *27 March 2020*
Accepted: *06 May 2020*
Published: *xx May 2020*

Citation:
Majkowska A, Redondo-Gómez C, Rice A, Gonzalez M, Inostroza-Brito KE, Collin E, Rodriguez-Cabello JC, Del Rio Hernandez AE, Solito E and Mata A (2020) Interfacial Self-Assembly to Spatially Organize Graphene Oxide Into Hierarchical and Bioactive Structures. Front. Mater. 7:167. doi: 10.3389/fmats.2020.00167

INTRODUCTION

Self-assembly, the process by which multiple smaller components autonomously interact and organize into larger well-defined structures, plays a crucial role in the way nature creates structure and functionality (Whitesides and Grzybowski, 2002). In an attempt to emulate biological systems, molecular self-assembly is being used to design bioinspired materials with a spectrum of exciting properties such as well-defined nanostructure (Zhang, 2003; Gazit, 2007), precise display of bioactive signals (Webber et al., 2010; Azevedo, 2019), temporal control of signaling (Kumar et al., 2018), and tuneable mechanical properties (Pashuck et al., 2010). Further processing has been used to enhance complexity for example via modulation of the assembly process (Zhang et al., 2010), top-down techniques (Mata et al., 2009; Mendes et al., 2013), or incorporation of multiple bioactive epitopes (Stephanopoulos et al., 2013; Gentile et al., 2017). However, the ability to assemble molecules hierarchically into well-defined macroscopic structures with practical use remains limited.

Multicomponent self-assembly offers an attractive route to design and engineer materials with molecular precision while increasing complexity and functionality (Draper et al., 2015). For example, the co-assembly of peptide amphiphiles (PAs) bearing either host or guest moieties has been recently used to develop hydrogels with enhanced mechanical properties (Redondo-Gómez et al., 2019). In a different approach, by co-assembling PAs with a megadalton hyaluronic acid, Capito et al. (2008) created stable sacs and membranes with hierarchical nano-to-micro structure. Inspired by this work, we have used PA molecules as self-assembling chaperones to interact with and guide the assembly of different types of molecules such as 1,3:2,4-dibenzylidene-D-sorbitol (DBS) gelators (Okesola et al., 2019), the protein resilin (Okesola et al., 2020a), or hyaluronan/nanoclay composites (Okesola et al., 2020b), generating hydrogels with tuneable structure and mechanical properties. Furthermore, taking advantage of hydrodynamic forces generated during additive manufacturing, Hedegaard et al. (2018) developed biocompatible hydrogel constructs with well-defined ordered or randomly oriented nanofibers, surface microtopographies, distinct microgeometries, and macroscopic assemblies.

Multicomponent self-assembly offers the possibility to not only take advantage of the properties of the individual components but also emergent assembling phenomena and synergistic properties (Okesola and Mata, 2018). In this context, Inostroza-Brito et al. (2015) demonstrated how PAs can affect the conformation of elastin-like recombinamers (ELRs) to consequently generate a diffusion-reaction assembly process. This mechanism enables the formation of a hierarchical multi-layered ELR5/PA membrane with the capacity to access non-equilibrium and a series of dynamic properties. While the resulting material is fragile (Inostroza-Brito et al., 2017), the study demonstrates the possibility to guide the assembly of complex components, such as proteins, beyond the nanoscale in a controllable and autonomous manner.

Graphene oxide (GO) is a single layer two-dimensional nanomaterial with a wide range of properties such as high surface area, mechanical strength, thermal conductivity, biocompatibility, and ease of functionalization (Zhu et al., 2010; Yang et al., 2013). Graphene-based materials have enormous potential in the biomedical field in applications ranging from biosensors (Justino et al., 2017) and biological imaging (Lin et al., 2016) to drug and gene delivery (Liu et al., 2013) and biomaterials (Shin et al., 2016). A variety of composite biomaterials incorporating a biomacromolecule and GO have been generated in the form of electrospun mats (Azarniya et al., 2016), hydrogels (Kang et al., 2015; Zhou et al., 2017), films (Han et al., 2011), or other 3D structures (Rajan Unnithan et al., 2017). For instance, nanocomposites of GO and chitosan have been prepared resulting in improved mechanical properties (Han et al., 2011; Li et al., 2013), resistance against enzymatic degradation (Shao et al., 2013), enhanced cellular (Depan et al., 2014; Dinescu et al., 2014), and antibacterial (Mazaheri et al., 2014) activity. Other GO-protein composite materials based on GO and gelatin or collagen have led to materials with improved mechanical properties (Wan et al., 2011; Jalaja et al., 2016) and bioactivity (Kang et al., 2015; Lee et al., 2016; Zhou et al., 2017). While these examples elucidate both the interest and progress of incorporating GO within biomaterials, the capacity to organize GO flakes hierarchically remains an unmet challenge.

Here, we report on the use of the ELR5/PA co-assembling system to enable localization and organization of GO flakes into hierarchical and functional structures. We demonstrate how the diffusion-reaction mechanism of formation can be used to guide the assembly of GO flakes between the ELR5/PA layers and generate complex geometries where GO is organized at multiple length scales. Furthermore, we reason that the assembly of GO in this manner will lead to enhanced mechanical properties of the ELR5/PA system. We describe the underlying mechanism of self-assembly, the structure of the composite material, and the biocompatibility of the resulting ELR5/PA/GO biomaterial through extensive *in vitro* cell studies.

RESULTS AND DISCUSSION

Rationale

The approach is based on the ELR5/PA co-assembling system (Inostroza-Brito et al., 2015, 2017) and takes advantage of its reaction-diffusion mechanism to recruit, localize, and organize GO flakes at multiple length scales (**Figure 1**). We used 0.04% (v/v) GO (Wick et al., 2014) (pH = 2) with monolayer content >95% and oxygen content >36% given its water dispersability and low cost (**Figure 1E**). We used a cationic PAK3 ($C_{15}H_{31}$CONH-VVVAAAKKK-$CONH_2$) to co-assemble with the oppositely charged ELR5 (MESLLP-[(VPGVG VPGVG VPGEG VPGVG VPGVG)$_{10}$-(VGIPG)$_{60}$]$_2$-[(VPGIG)$_{10}$-AVTGRGDSPASS(VPGIG)$_{10}$]$_2$-V) molecule to evaluate the capacity of the assembling process to recruit and organize GO flakes within the distinctive ELR5/PA multilayers (**Figure 1A**). Furthermore, given our previous findings that distinct PA molecules can generate different ELR5/PA membrane structures (Inostroza-Brito et al., 2015), PAs with different charge densities including PAK2 ($C_{15}H_{31}$CONH-VVVAAAKK-$CONH_2$) and PAK4 ($C_{15}H_{31}$CONH-VVVAAAKKKK-$CONH_2$) were also used to co-assemble with ELR5 (**Figure 1D**). In addition, the resulting materials were characterized according to their mechanical properties and used as cell culture substrates to investigate their effect on cell adhesion, proliferation, metabolic activity, and morphology.

Synthesis of Individual Components

PA molecules were synthesized following standard solid-phase peptide synthesis methods as previously reported (Mata et al., 2012). PA purity and structural conformation was characterized by reverse phase HPLC and electrospray ionization mass spectrometry (Figure S1). ELR5 molecules were obtained from Technical Proteins Nanobiotechnology S. L., Spain and GO aqueous dispersions were obtained from Sigma Aldrich, UK.

Characterization of Interactions Between Components

The ELR5/PA system relies on electrostatic, hydrophobic, and H-bond interactions (Inostroza-Brito et al., 2015). Consequently, we

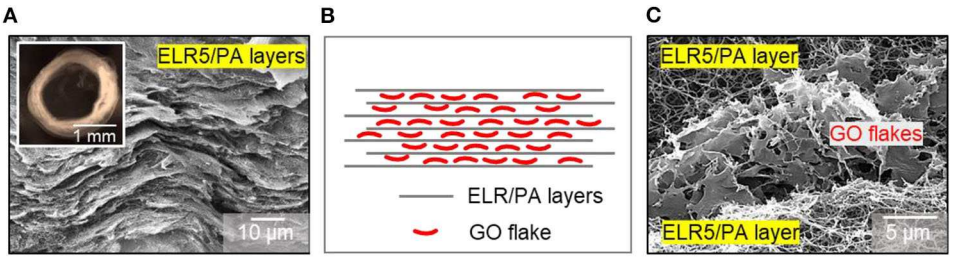

D

MOLECULE	SEQUENCE	M_w (kDa)
PAK2	$C_{15}H_{31}$CONH-VVVAAAKK-$CONH_2$	1.022
PAK3	$C_{15}H_{31}$CONH-VVVAAAKKK-$CONH_2$	1.150
PAK4	$C_{15}H_{31}$CONH-VVVAAAKKKK-$CONH_2$	1.279
ELR5	MESLLP-$[(VPGVG\ VPGVG\ VPGEG\ VPGVG\ VPGVG)_{10}$-$(VGIPG)_{60}]_2$-$[(VPGIG)_{10}$-AVTGRGDSPASS$(VPGIG)_{10}]_2$-V	112.300

E GRAPHENE OXIDE

pH 2

Lateral size: 7 ± 2 µm

Monolayer content: ≥ 95 %

Zeta potential: -30.58 mV

Oxygen content: ≥ 36%

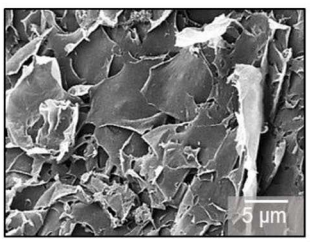

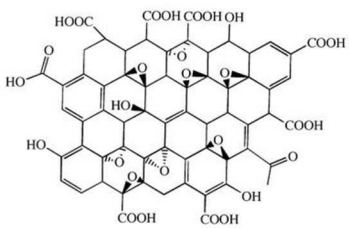

FIGURE 1 | Schematic representation and representative images of tubes and tube wall cross-sections of the ELR5/PA/GO system. **(A)** SEM micrograph of an ELR5/PA cross-section with its characteristic multi-layered architecture. Inset: Bright field image of a top view of an ELR5/PA tube. **(B)** Schematic of the ELR5/PA system cross-section with black horizontal lines representing ELR5/PA layers embedded with GO flakes (red). **(C)** SEM micrograph of the cross-section of an ELR5/PA/GO membrane visualizing the localization of GO flakes between ELR5/PA layers. **(D,E)** Molecular structure information of PAs, ELR5, and GO used in this work.

first used circular dichroism (CD) to investigate the secondary structure in aqueous solution of both PAs and ELR5 with and without GO. CD revealed that PAK3 exists in a random coil conformation when dissolved in MilliQ™ water at pH 4.5 and room temperature (RT), and does not undergo conformational change when mixed with GO under the same conditions (**Figure 2A**). However, a slight red-shift at the 195 nm minimum was observed, which might indicate an interaction between PAK3 and GO as previously reported (Pashuck et al., 2010). CD on ELR5 samples dissolved in MilliQ™ water at pH 5 and RT exhibited both random coil and β-sheet conformations (**Figure 2A**) that did not change upon addition of GO. However, lower intensity of the negative 195 nm signal might indicate that GO reduces the content of random coil structures in ELR5 while increasing the content of type I β-turns (Perczel and Fasman, 1992).

We further investigated the ELR5/PA/GO interactions by conducting zeta potential and dynamic light scattering (DLS) measurements. zeta potential of PAK3 decreased after addition of GO (**Figure 2B**). This is likely a consequence of a drop in the PAK3's surface charge as a result of its electrostatic interactions with carboxyl, hydroxyl, or carbonyl groups present in GO (negatively charged), partially screening the positive charges of PAK3. On the other hand, the zeta potential of ELR5 molecules increased slightly after addition of GO, suggesting absence of electrostatic interactions between these components, which is in agreement with the CD results (**Figure 2A**). DLS measurements revealed a dramatic decrease in GO size after mixing with both PAK3 (**Figure 2C**) and ELR5, which suggests disruption of GO aggregates, known to form in aqueous solutions (Tang et al., 2015), due to electrostatic interactions. It is important to mention that DLS is a well-suited technique for estimating the size of spherical particles. However, this technique has been also used to provide relative changes in size of non-spherical components including GO (Stankovich et al., 2006), Pas (Raymond and Nilsson, 2018), and ELRs (Navon and Bitton, 2016).

Hydrophobic interactions also play a key role in the ELR5/PA system above the ELR5's transition temperature (Tt) (Inostroza-Brito et al., 2015). To investigate whether addition of GO into the ELR5/PA system influences hydrophobic interactions, a turbidity

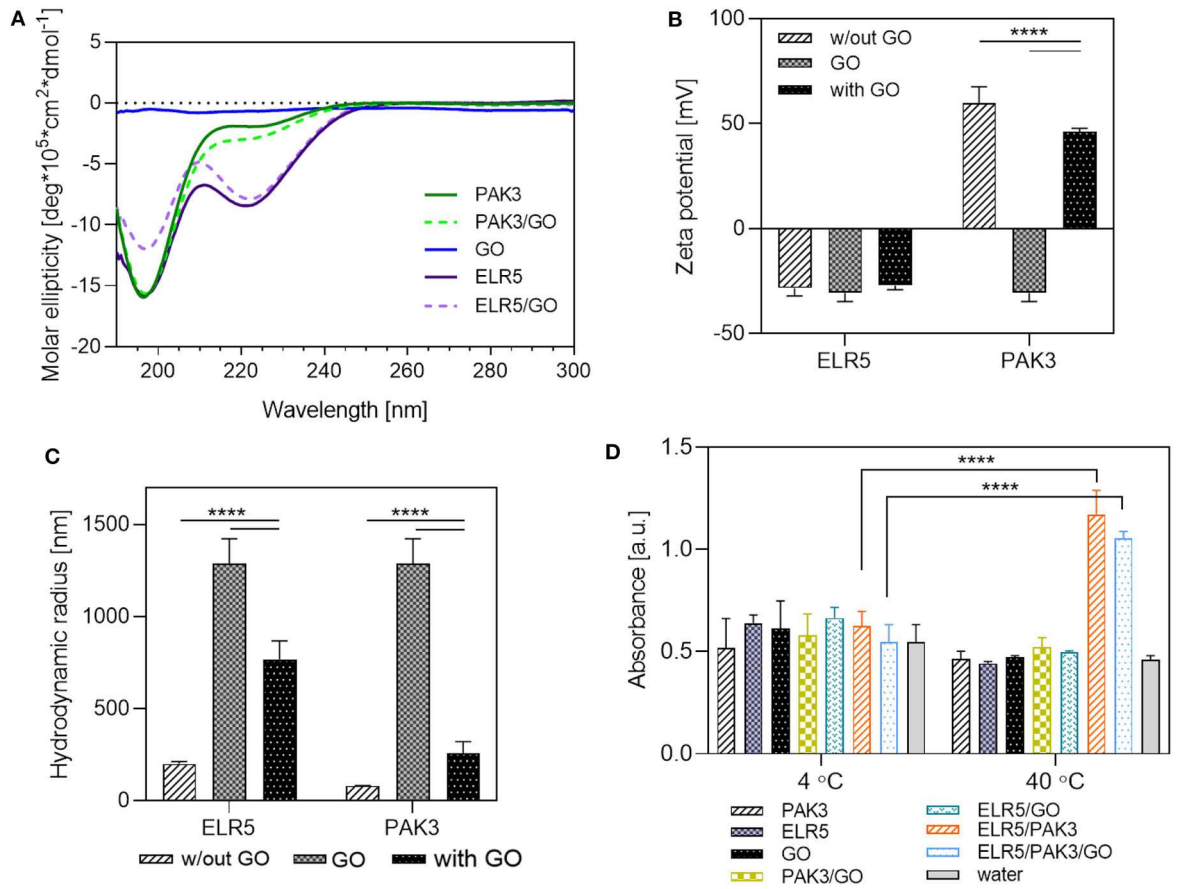

FIGURE 2 | Analysis of interactions between PAK3, ELR5, and GO. **(A)** CD spectra of PAK3, ELR5, and their mixtures with GO in aqueous solutions at room temperature. **(B)** Zeta potential measurements of aqueous solutions of PAK3, ELR5, and their mixtures with GO. **(C)** DLS measurements of aqueous solutions of PAK3, ELR5, and their mixtures with GO **(D)** Turbidity of aqueous solutions of PAK3, ELR5, and their mixtures with GO at 4 and 40°C measured at 300 nm. Error bars represent ±SD where ****$p < 0.0001$ and ***$p < 0.001$. The experiments were performed in triplicates.

assay was performed. The results confirmed that significant levels of aggregation between ELR5, PAK3, and GO are only present when the temperature is above the Tt of ELR5 (**Figure 2D**), which indicates that presence of GO in the solution does not influence the hydrophobic interactions between PAK3 and ELR5, necessary for membrane formation (Inostroza-Brito et al., 2015).

These results indicate that molecular interaction between GO and both molecular building blocks (PAK3 and ELR5) relies mostly on electrostatic forces. However, both components retain most of their secondary structures in presence of GO and, consequently, hydrophobic interactions from ELR5 seem to also play a key role above the ELR5 transition temperature.

The ELR5/PA/GO Membrane—Micro and Macroscopic Properties

Upon ELR5/PAK3 co-assembly, a diffusion barrier is formed across which the PAK3 diffuses (Inostroza-Brito et al., 2015). Electron microscopy was used to investigate the assembly of GO within the ELR5/PAK3 membrane when added into the system. We first mixed GO with the PAK3 solution and subsequently inoculated it into the ELR5 solution. Scanning electron microscopy (SEM) revealed poor incorporation of GO (**Figure 3B**), likely as a result of the inability of the relatively large GO flakes to diffuse through the ELR5/PAK3 diffusion barrier. We then reasoned that combining GO with ELR5 solution might surpass this obstacle. We prepared an ELR5/GO solution followed by inoculation of PAK3 into the mixture. In this case, we observed much higher incorporation of GO in the final membrane (**Figure 3C**). Given these findings, we then mixed GO with both ELR5 and PAK3 solutions, followed by inoculation of PAK3/GO in the ELR5/GO solution. In this setup, membranes qualitatively exhibited the highest incorporation of GO (**Figure 3D**) while maintaining their multi-layered structure and capacity to adhere to interfaces and open controllably, transforming sacs into tubular structures (**Figures 4C–E**) (Supplementary Information). Transmission electron microscopy (TEM) revealed presence of GO flakes (visible as black lines) throughout the thickness of the ELR5/PAK3/GO membrane, positioned within and parallel to the membrane layers (**Figure 4B**). SEM performed on the membranes confirmed the multi-layered microarchitecture with embedded GO flakes (**Figure 3F**-row) seen on TEM. These

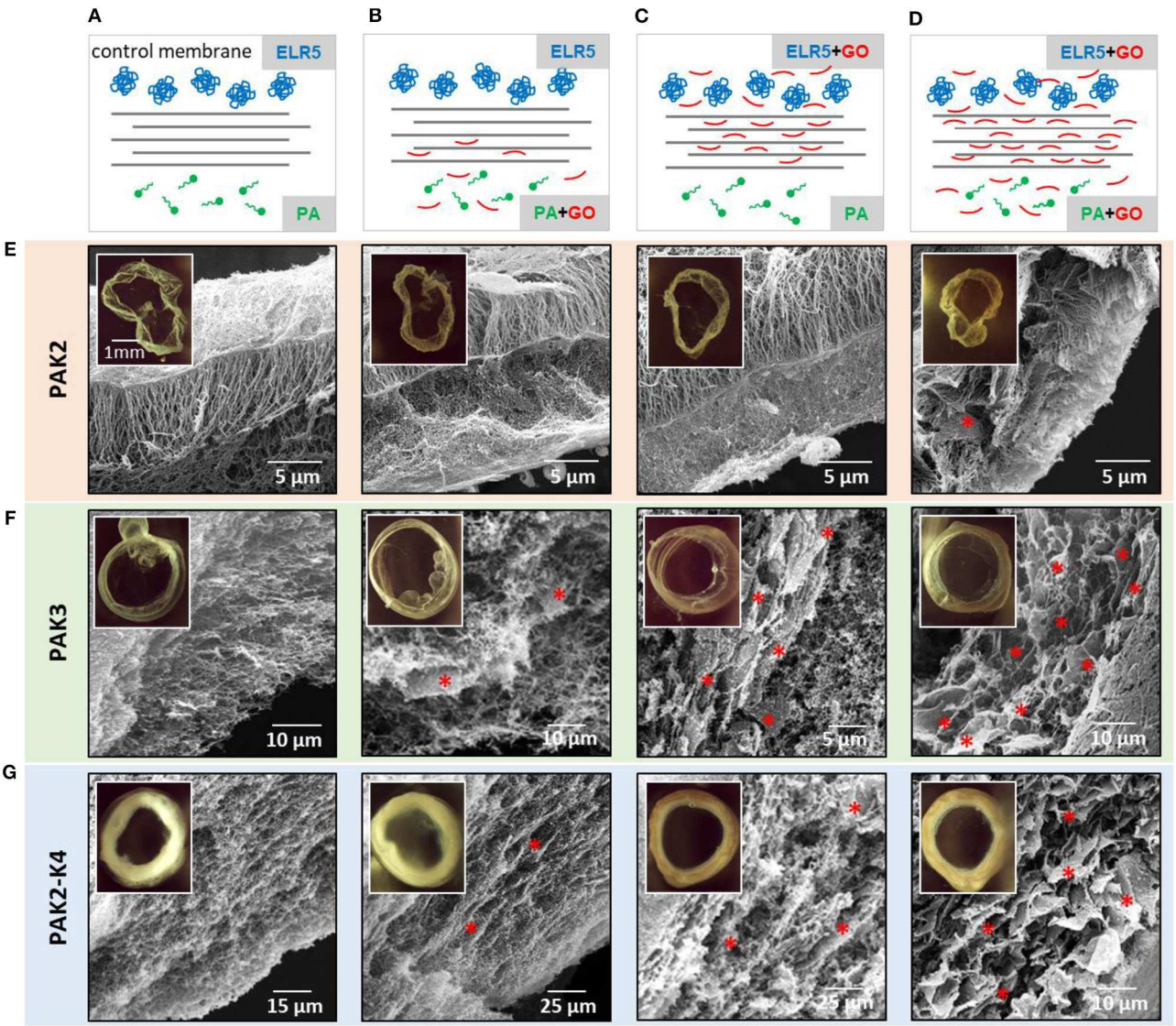

FIGURE 3 | Investigation of GO incorporation in different ELR5/PA systems. First row illustrates the different experimental setups including **(A)** co-assembly of ELR5 and PAK3 (control), **(B)** GO combined with PAs before membrane formation, **(C)** GO combined with ELR5 before membrane formation, and **(D)** GO combined with both PAs and ELR5 before membrane formation. Rows **(E,F,G)** depict SEM micrographs of cross-sections of the different systems including ELR5/PAK2 (row **E**), ELR5/PAK3 (row **F**), and ELR5/PAK2-K4 (row **G**). Asterisks * point to GO flakes. Insets are top view bright field images of the corresponding tubes. Differences in color/contrast of the inset images are a result of differences in the structure of the generated membranes.

results indicate that GO can be successfully incorporated within the ELR5/PAK3 system by taking advantage of the diffusion-reaction mechanism of assembly to recruit, localize, and organize GO flakes within the multi-layered architecture and as part of a more complex geometrical structure.

Incorporation Studies

To investigate the possibility to use supramolecular self-assembling processes to guide the organization of GO more broadly, we repeated the experiments using variations of PAK3, PAK2 (C15H31-VVVAAAKK–CONH2) and PAK4 (C15H31-VVVAAAKKKK-CONH2) (**Figure 1D**). We have previously demonstrated that these PA molecules with a different number of lysine residues were also able to form stable ELR5/PA membranes, but exhibiting different cross-sectional architectures (Inostroza-Brito et al., 2015). Membranes formed using PAK4 exhibited a multi-layered architecture with increased thickness and a looser structure compared to ELR5/PAK3 membranes (Inostroza-Brito et al., 2015) while those formed using PAK2 exhibited a different three-level structure with orthogonal fibers (**Figure 3F**-row) (Inostroza-Brito et al., 2015). To study the interaction between GO and the ELR5/PAK2-K4 system, we also attempted to generate ELR5/PA membranes combining both PAK2 and PAK4 (1:1 mixture). We hypothesized that the

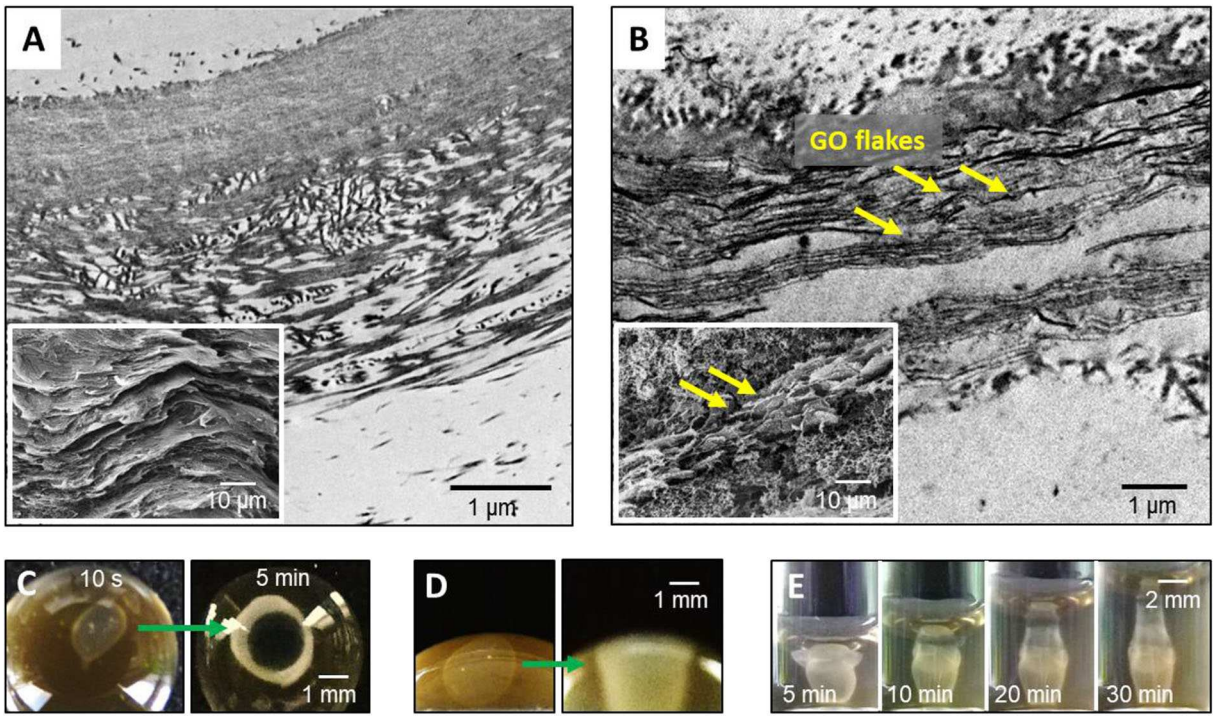

FIGURE 4 | Investigation of GO incorporation and ELR5/PAK3/GO membrane properties. **(A)** TEM micrograph of a cross-section of an ELR5/PAK3 membrane (Inset is a representative SEM micrograph). **(B)** TEM micrograph of a cross-section of an ELR5/PAK3/GO membrane with GO flakes (yellow arrows) (Inset is a representative SEM micrograph). **(C–E)** Demonstration of the dynamic properties of the ELR5/PAK3/GO system including spontaneous opening after a drop of PAK3/GO solution is inoculated into an ELR5/GO solution **(C–E)** capacity for longitudinal growth upon increasing the ELR5/GO volume.

different diffusion mechanisms arising from the co-assembly of these different components would guide and organize GO flakes differently. To investigate this hypothesis, experiments were conducted using ELR5/PAK2 and ELR5/PAK2-K4 combinations (**Figures 3E,G**-rows). As before, GO was mixed with (i) PAs alone, (ii) ELR5 alone, and (iii) both components (**Figures 3B–D**). ELR5/PAK2/GO and ELR5/PAK2-K4/GO membranes were stable and robust (**Figures 3E,G** insets) and exhibited darker color suggesting GO incorporation in these conditions, which was assessed by observations under an optical microscope. SEM investigations on membranes revealed GO flakes were incorporated and organized within and throughout the multi-layered architecture of the ELR5/PAK2-K4/GO membranes (**Figure 3G**-row). As with the ELR5/PAK3/GO system, highest incorporation of GO was achieved when the GO was mixed with both PA and ELR5 solutions (**Figures 3D,F**). In contrast, ELR5/PAK2/GO membranes exhibited large quantities of GO on the outer and inner side of the membrane but only marginal incorporation within the membrane.

These results suggest that GO can be incorporated within the ELR5/PA system independently of the PA molecule used. However, the level of incorporation of GO within the membrane depends on the supramolecular mechanism of assembly, with both ELR5/PAK3/GO and ELR5/PAK2-K4/GO presenting more GO in the multilayers than ELR5/PAK2/GO membranes, which present a different mechanism of co-assembly (Inostroza-Brito et al., 2015). Initial formation of a diffusion barrier prevents large flakes of GO from diffusing through the barrier, forming membranes with less GO flakes. Addition of GO flakes in the ELR5 solution helps to overcome this obstacle, forming membranes with higher content of GO. Highest incorporation, however, can be achieved only when GO is combined with both PA and ELR5 solutions, particularly in the case of the ELR5/PAK3 and ELR5/PAK2-K4 systems.

Membrane Thickness

To study the effect of introducing GO into the ELPR5/PA system, possible changes in membrane thickness were investigated by SEM (**Figure 5B**). SEM revealed that the thickness of ELR5/PAK3/GO membranes increased when GO was added in either PA or ELR5 solutions prior to assembly, forming the thickest membrane when GO was mixed with both ELR5 and PAK3 (**Figure 5D**). Similar results were observed in ELR5/PAK2-K4/GO membranes (**Figure 5D**). In contrast, the thickness of ELR5/PAK2/GO membranes gradually decreased with addition of GO to either PAK2, ELR5, or both PAK2 and ELR5 solutions. This result suggests that the supramolecular mechanism of assembly of ELR5/PAK2 membranes, which differs from ELR5/PAK3 and ELR5/PAK4 systems (Inostroza-Brito et al., 2015), prevents incorporation of GO. These experiments are in alignment with the SEM observations (**Figure 3**) and confirm that, while supramolecular processes may be able

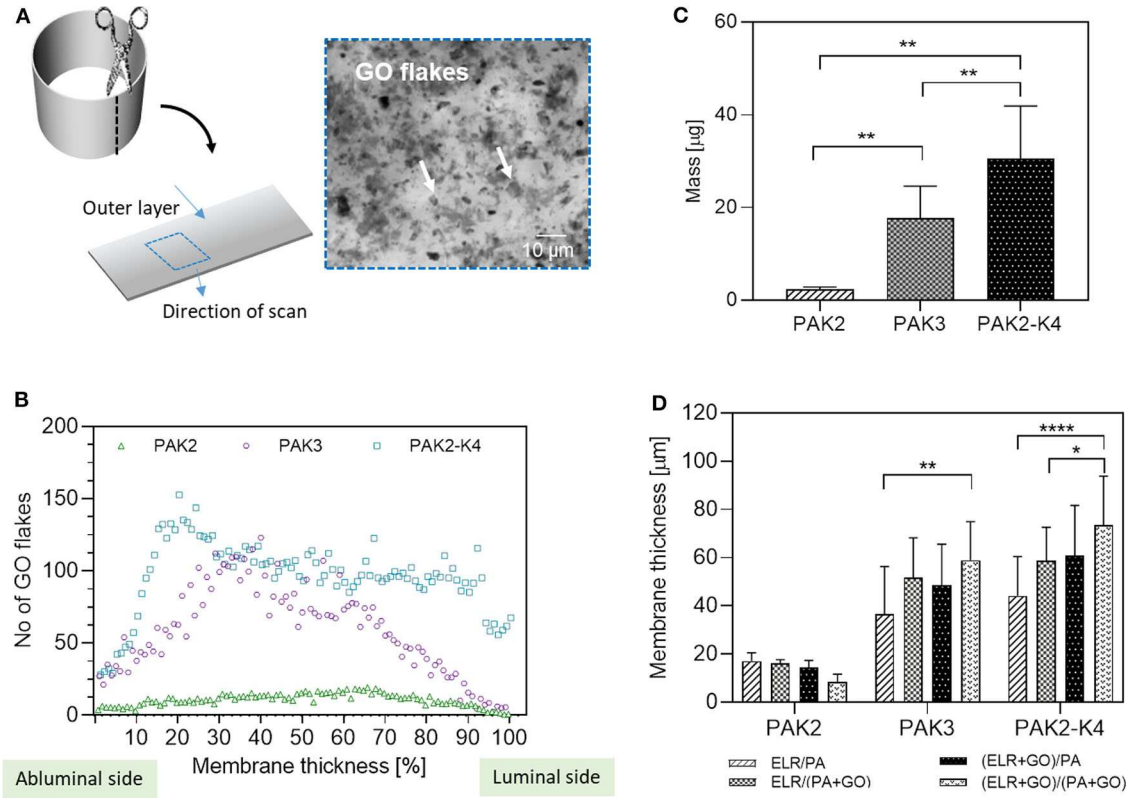

FIGURE 5 | GO content and distribution in the membranes. **(A)** Schematic of the experimental setup for measuring GO distribution. **(B)** GO distribution profile throughout the thickness of the ELR5/PAs/GO systems. Number of GO flakes present in each layer of a z-stack image was quantified and presented as number of GO flakes vs. layer number which was normalized as % of the thickness of the membrane. **(C)** GO content per membrane as measured by UV-Vis. **(D)** Thickness of the membranes as measured by SEM. Error bars represent ±SD where ****$p < 0.0001$, ***$p < 0.001$, **$p < 0.01$, and *$p < 0.5$. The experiments were performed in triplicate.

to organize GO flakes at multiple scales (ELR5/PAK3 and ELR5/PAK2-K4 systems), the size of GO flakes may limit its incorporation in some co-assembling systems (ELR5/PAK2).

GO Content

To further characterize GO incorporation, the amount of GO within each of the ELR5/PA systems was quantified. After co-assembly, membranes were dissolved in 1,1,1,3,3,3-Hexafluoro-2-propanol (HFIP) and GO absorbance was monitored spectrophotometrically in the UV-Vis region. The technique enabled quantification of mass of GO per membrane (**Figure 5C**) and the results revealed the highest incorporation of GO occurred in ELR5/PAK2-K4 membranes, followed by ELR5/PAK3 membranes, and, as expected, ELR5/PAK2 membranes with the lowest incorporation of GO. These results correlate with the previously discussed SEM observations (**Figure 3**) and membrane thickness experiments (**Figure 5B**).

Distribution of GO

SEM and TEM demonstrated that GO flakes are incorporated and organized within the ELR5/PAK3/GO and ELR5/PAK2-K4/GO membranes. To further characterize the level of incorporation throughout the thickness of the membrane, 3D z-stacked bright field images of the membrane were generated (**Figure 5A**). Using ImageJ software (Schneider et al., 2012), we quantified the number of GO flakes in each layer of the different membranes by generating z-stack images and producing distribution profiles depicting number of GO flakes vs. layer number, which was normalized as % of the thickness of the membrane (**Figure 5B**). These profiles revealed that in ELR5/PAK3/GO membranes, GO is distributed throughout the thickness of the membrane with higher amounts present in the middle. In addition, ELR5/PAK2-K4/GO membranes exhibited similar level of GO incorporation but the flakes were more evenly distributed throughout the membrane (**Figure 5B**). Interestingly, ELR5/PAK2/GO membranes exhibited uniform distribution throughout the membrane but with much lower levels of incorporation (**Figure 5B**). These results confirm that GO flakes were in fact distributed throughout the membranes of all the systems studied but with different levels of incorporation. Highest incorporation and distribution was observed in ELR5/PAK2-K4/GO and ELR5/PAK3/GO membranes, on which we focused to assess applicability.

Mechanical Properties of the ELR5/PA/GO Systems

Given the unique mechanical properties of GO (Zhu et al., 2010) as well as its incorporation and organization within the ELR5/PA systems, we hypothesized that the mechanical properties of the resulting ELR5/PA/GO membranes would improve compared to the control ELR5/PA membranes. Atomic force microscopy (AFM) measurements were conducted on both luminal (inner) and abluminal (outer) sides of ELR5/PAK3/GO and ELR5/PAK2-K4/GO membranes assembled with GO added to both PA and ELR5 solutions (**Figure 6**). The results revealed significant increase in Young's Moduli of the ELR5/PAK2-K4/GO membrane on both luminal and abluminal sides compared to ELR5/PAK2-K4 membranes (**Figure 6B**). This increase was also evident in ELR5/PAK3/GO membranes compared to ELR5/PAK3 ones (**Figure 6A**). These results suggest that stiffness of the ELR5/PA membrane increases after incorporation of GO on both sides of the membrane, which correlates with the SEM observations (**Figure 3**), membrane thickness measurements (**Figure 5C**), and GO distribution and incorporation (**Figure 5D**) within the membrane's microstructure when GO is added to both ELR5 and PAs solutions.

Cell Studies

Cell Adhesion

The potential applicability of the ELR5/PA/GO materials was investigated by assessing the suitability of the membrane to be used in tissue engineering applications. Mouse adipose derived stem cells (mADSCs) were cultured on both sides of the membranes that presented higher incorporation of GO including ELR5/PAK3, ELR5/PAK3/GO, ELR5/PAK2-K4, and ELR5/PAK2-K4/GO. Preliminary biocompatibility was assessed by quantifying cell adhesion, viability, and proliferation.

mADSCs were seeded on both ELR5/PAK3 and ELR5/PAK2-K4 membranes (with and without GO) in serum-free media, incubated for 4 h, rinsed to remove non-adherent cells, cultured for an additional 4 h in full media (DMEM, 20% FBS), and then dyed with the blue dsDNA stain 4'-6-diamino-2-phenylindole (DAPI). Fluorescent microscopy revealed higher numbers of cells growing on ELR5/PAK3 and ELR5/PAK3/GO membranes than on ELR5/PAK2-K4 and ELR5/PAK2-K4/GO membranes (**Figure 7B**). To verify these results, we quantified the amount of double strand DNA (dsDNA) present in the samples by PicoGreen™ assay. This assay allows the quantification of the concentration of dsDNA that can be interpreted as proportional to the number of cells present in the sample. mADSCs from membranes were collected after 7 days of culture and tissue culture plate (TCP) was used as control. The results revealed similar dsDNA concentration of cells growing on ELR5/PAK3 and ELR5/PAK3/GO membranes, suggesting that these membranes facilitate cell adhesion and proliferation (**Figure 7A**). In contrast, dsDNA concentration of cells growing on both ELR5/PAK2-K4 and ELR5/PAK2-K4/GO membranes was significantly lower than TCP. We hypothesize that the decrease in cellular dsDNA may be the result of (i) a greater cytotoxic effect from the positives charges of PAK4 (Newcomb et al., 2014) or (ii) the higher Young's Modulus of both ELR5/PAK2-K4 and ELR5/PAK2-K4/GO (compared to ELR5/PAK3 and ELR5/PAK3/GO; **Figure 6**), which could influence cell adhesion. Previous studies have demonstrated that stiffer surfaces can result on lower mADSCs adhesion (Discher et al., 2005).

In summary, these results reveal that incorporation of GO within both ELR5/PAK3 and ELR5/PAK2-K4 systems does not affect the biocompatibility of the material but differences in the resulting architecture and material properties may lead to differences in the capacity of the material to promote cell adhesion and proliferation.

Cell Morphology

Cells stained with DAPI (nucleus) and Phalloidin CruzFluor™ 647 (actin) were imaged under an epifluorescent microscope. Analysis of the stained cells revealed that cells grown on ELR5/PAK3 and ELR5/PAK3/GO membranes exhibited a well-spread morphology and formed multiple connections with surrounding cells (**Figure 7E**). In contrast, cells grown on ELR5/PAK2-K4 and ELR5/PAK2-K4/GO membranes displayed a much less spread morphology and formed fewer connections with neighboring cell. These results suggest that ELR5/PAK3 membranes support better cell adhesion compared to ELR5/PAK2-K4 membranes regardless of the GO content.

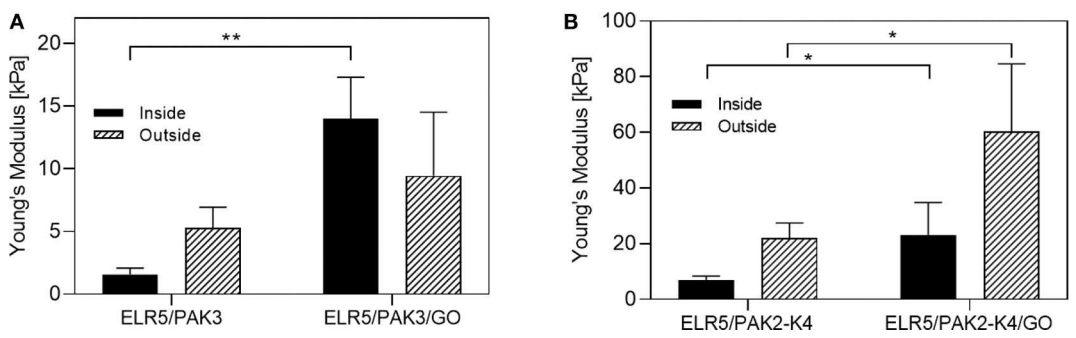

FIGURE 6 | Young's Moduli of the membranes. AFM measurements were carried out on the luminal (inner) and abluminal (outer) side of the ELR5/PAK3 ± GO membranes **(A)** and ELR5/PAK2-K4 ± GO membranes **(B)**. Error bars represent ±SEM where $^{**}p < 0.01$, and $^{*}p < 0.5$. The experiments were performed in 5 replicates.

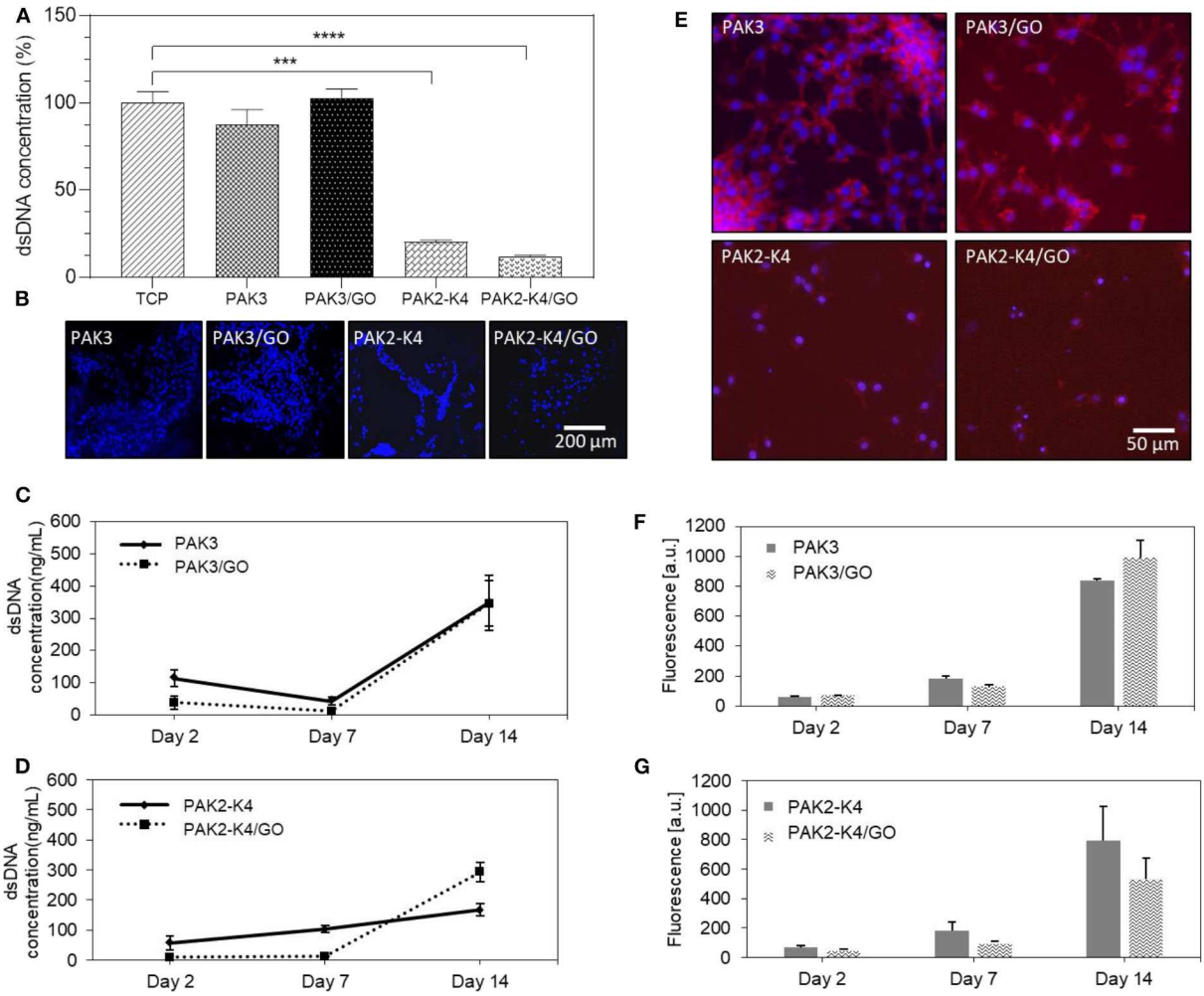

FIGURE 7 | Investigation of biocompatibility of ELR5/PAs/GO membranes. Mouse derived adipose stem cells (mADSCs) were grown on the membranes and dsDNA content **(A)** was quantified after 7 day in culture and normalized to TCP (100%) by PicoGreen™ assay. **(B)** Fluorescence microscopy images of mADSCs stained with DAPI (4,6-diamidino-2-phenylindole) after 4 h of cell culture. **(C,D)** Proliferation studies. mADSCs were grown on the ELR5/PAK3 ± GO **(C)** or ELR5/PAK2-K4 ± GO **(D)** membranes. dsDNA content was quantified by PicoGreen™ assay. **(E)** Morphology studies. mADSCs were stained with Phalloidin CruzFluor™ 647 and DAPI. Images indicate a spreading morphology and intercellular connections between mADSCs growing on ELR5/PAK3 and ELR5/PAK3/GO membranes and a barely visible cytoskeleton of mADSCs grown on ELR5/PAK2-K4 and ELR5/PAK2-K4/GO membranes with minimal spreading and connections observed. **(F,G)** Cell metabolic activity studies. mADSCs were grown on the ELR5/PAK3 ± GO **(F)** or ELR5/PAK2-K4 ± GO **(G)** membranes, cell metabolic activity was assessed with Alamar Blue™ assay. The data suggest there is no significant difference in cell metabolic activity between either ELR5/PAK3 and ELR5/PAK3/GO nor ELR5/PAK2-K4 and ELR5/PAK2-K4/GO systems at any of the time points. Error bars represent ±SD where $^{****}p < 0.0001$, $^{***}p < 0.001$, $^{**}p < 0.01$, and $^{*}p < 0.5$. The experiments were performed in triplicates.

Cell Metabolic Activity

To further assess the capacity of the materials to support cell growth, the metabolic activity of mADSCs on the membranes was assessed by Alamar blue™ assay over 2 weeks of cell culture. Same membranes used for cell adhesion studies (**Figure 7E**) revealed no significant difference in metabolic activity for cells growing on the ELR5/PAK3/GO membranes vs. ELR5/PAK3 membranes at any time point (**Figure 7F**). On the other hand, cells grown on ELR5/PAK2-K4/GO membranes exhibited a slight decrease, though not statistically significant, in metabolic activity compared to those grown on ELR5/PAK2-K4 membranes. These results further evidence that addition of GO flakes into the ELR5/PAK3 system does not have a negative impact on the metabolic activity of the cells. However, there is a slight decrease in cell metabolic activity after addition of GO in the ELR5/PAK2-K4 system, suggesting supramolecular organization of GO within the membranes or the possible cytotoxicity of the positively charged PAK4 (Newcomb et al., 2014) might play a role.

Cell Proliferation

Cell proliferation was then assessed by quantifying dsDNA concentration of mADSCs grown on the different membranes on days 2, 7, and 14 via Quant-iT™ PicoGreen™ assay. The results revealed that in case of the ELR5/PAK3 system, GO

does not have an effect on the proliferation of mADSCs at none of the investigated time points (**Figure 7C**). On the other hand, we observed that GO may be influencing proliferation of mADSCs grown on ELR5/PAK2-K4 membranes, given a decrease in dsDNA concentration at day 7 and an increase at day 14 compared to membranes without GO (**Figure 7D**). These results indicate that both ELR5/PAK3 and ELR5/PAK2-K4 systems support cell proliferation regardless of GO content, although, proliferation rate is slower for cells growing on the ELR5/PAK2-K4 system.

CONCLUSION

In this study, we report the ability of the ELR5/PA self-assembling system to manipulate, localize, and organize GO flakes into hierarchical structures. By taking advantage of the electrostatic and hydrophobic nature of ELR5 and PAs, the formation of a diffusion barrier upon their co-assembly, and the subsequent diffusion-reaction mechanism of ELR5/PA membrane formation, we demonstrate the potential to use supramolecular mechanisms to guide assembly of GO across scales and into complex architectures. Furthermore, we show that incorporation of GO flakes within the ELR5/PA system improves mechanical properties of the resulting materials and may be beneficial for tissue engineering applications. Also, we demonstrate that incorporation of GO does not affect the capacity of the composite material to support mADSCs adhesion, proliferation, and metabolic activity.

METHODS

Membrane Formation

ELR5 and PA molecules were dissolved separately in MilliQ water (10 and 15 mg/mL, respectively). pH was adjusted to pH = 5 (ELR5) and pH = 4.5 (PAs). One hundred and ninety microliter of ELR5 solution was placed in a well in a 48 well plate. Ten microliter of PA solution was added by immersing the pipette tip into the ELR5 solution and slowly releasing the liquid. The membrane was left to develop for 48 h at 30°C. For GO membranes: GO 4 mg/mL (pH = 2) was diluted to the required concentration with pH adjusted to pH = 4.5 and mixed with either ELR5 solution or PA solution before membrane formation. Ten microliter of PA-GO solution was added by immersing the pipette tip into the ELR5-GO solution and slowly releasing the liquid. The membrane was left to develop for 48 h at 30°C.

Growth Experiment

ELR5 and PA molecules were dissolved separately in MilliQ water (10 and 15, mg/mL respectively). GO 4 mg/mL was diluted to the required concentration and mixed with either ELR5 solution or PA solution before membrane formation. Hundred microliter of ELR5/GO solution was placed in a glass vial. Five microliter of PA-GO solution was added by immersing the pipette tip into the ELR5 solution and slowly releasing the liquid. Additional 20 μl of ELR5/GO solution was carefully added to the vial every 10 min to observe growth of the membrane.

Zeta Potential and Dynamic Light Scattering

Zeta potential was measured to investigate the changes in surface charge density of ELR5, PA and GO molecules when mixed together. ELR5 and PA were dissolved in MilliQ water [0.1 and 0.15% (w/v), respectively]. GO was diluted to the final concentration of 0.001% (w/v). pH was adjusted to pH = 5 (ELR5) and pH = 4.5 (PAs), and pH = 4.5 (GO). All samples were sonicated for 30 min prior taking the measurement. Zeta potential was measured at 25°C on a Zetasizer (Nano-ZS ZEN 3600, Malvern Instruments, UK).

Circular Dichroism Spectroscopy

ELR5 and PAs were dissolved in MilliQ water [0.025 and 0.01% (w/v), respectively]. In order to carry out the measurement at the same conditions as membrane formation, pH was adjusted to pH = 5 (ELR5) and pH = 4.5 (PAs). GO was diluted to the final concentration of 0.001% (w/v) and pH was adjusted to pH = 4.5. CD spectra were obtained using 1 mm path length and 300 μl volume quartz cuvette (Chirascan, Applied Photophysics, UK). between 195 and 270 nm with a 0.5 nm interval at 25°C. CD measurement was conducted using Chirascan™ CD spectrometer (Chirascan, Applied Photophysics Ltd, UK) equipped with a Peltier temperature controller, under a constant nitrogen purging at a constant pressure of 0.7 MPa. Each represented spectrum is the average of three consecutive spectra.

Turbidity

ELR5 and PA were dissolved in MilliQ water [0.025 and 0.01% (w/v), respectively]. GO was diluted to the final concentration of 0.001% (w/v). Absorbance of the solutions was measured at 300 nm using a microplate reader (Spetrostarnano, BMG Labtech, UK) at 4 and 40°C.

Transmission Electron Microscopy

Membranes were formed as described. After washing with MilliQ water membranes were crosslinked with TEM grade glutaraldehyde followed by dehydration with a gradient 30–100% of ethanol. Membranes were then embedded on LRWhite resin and ethanol 50–50% for 1 h and 100% LRW 1 h and again 100% LRW overnight. The following day they were encased in capsules filled with resin and left in the oven at 60°C for 5 h to harden. The block was sectioned with a Reicht microtome to a thickness of 70 nm. The sections were loaded onto a copper grid and stained with 2% uranyl acetate for 4 min and rinsed in MilliQ water. The samples were visualized on a JEOL JEM 1230 electron microscope operating at 80 kV.

Scanning Electron Microscopy

ELR5/PA/GO membranes were left to develop for 48 h and then washed in MilliQ water and fixed with 2.5% glutaraldehyde in MilliQ water for 2 h at room temperature. Then, the samples were washed in MilliQ water followed by dehydration by immersion in an increasing concentration of ethanol (20, 50, 70, 90, 96, and 100%). The samples were then subjected to a process of critical point drying (K850, Quorum Technologies, UK) followed by

sputter-coating with gold for 90 s. SEM imaging was carried out using an Inspect F50 (FEI Comp, The Netherlands).

GO Distribution

Membranes were formed as previously described. After washing in MilliQ water membranes were cut open, put flat on a microscope slide and then covered with a slide cover. 3D images were obtained with Zeiss LSM710 confocal microscope.

GO Mass

Fully formed and washed membranes were dissolved in 1,1,1,3,3,3-Hexafluoro-2-propanol (HFIP) followed by sonication for 30 min. GO absorbance was measured spectrophotometrically in the UV-VIS region. Standard curve was prepared using a solution of GO flakes in hexafluoroisopropanol at a known concentration.

Atomic Force Microscopy

Atomic force microscopy was used to measure Young's Modulus of the investigated system. Membranes were attached to a Petri dish using a drop of cyanoacrylate adhesive and left for a minute for the adhesive to dry followed by immersion in ultrapure MilliQ water. Young's Modulus measurements were taken with JPK Nanowizard-1 (JPK Instruments, Germany) in force spectroscopy mode, which was mounted on an inverted optical microscope (IX-81, Olympus, Japan). Indentation was carried out using quadratic pyramidal cantilevers (MLCT, Bruker, MA, USA) with spring constant of 0.07 N/m and half-angle to face of 17.5°. Measurements were taken in multiple areas per sample and multiple times per area.

Cell Studies

Fully developed membranes were washed with MilliQ water and crosslinked with genipin at a concentration of 25 μl/ml at 37°C overnight. Tubes were then washed in MilliQ water and sterilized under UV light for 20 min. After sterilization, tubes were washed three times in Hank's balanced salt solution. Fifty thousand mADSCs re-suspended in DMEM (10%FBS, 1%P/S) were seeded on each ELR5/PA/GO tube. Media was changed every 2 to 3 days.

Cell Attachment

Cells were seeded as previously described in a serum free DMEM media and incubated for 4 h followed by additional 4 h in full media (DMEM with 20% FBS). Cells were fixed with 4% paraform aldehyde for 1 h and stained with blue dye 4'-6-diamino-2-phenylindole (DAPI), followed by imaging under an epifluorescent microscope (Leica DMi8).

Cell morphology was assessed by using epifluorescent microscopy (Leica DMi8). After the cell culture membranes were fixed with 4% paraform aldehyde for 1 h and stained with 4'-6-diamino-2-phenylindole (DAPI) and Phalloidin CruzFluor™ 647.

Cell metabolic activity was assessed on days 2, 7, and 14 with AlamarBlue™ cell metabolic assay. Membranes were incubated for 2 h at 37°C in a 10% (v/v) solution of AlamarBlue™ in DMEM. Fluorescence of the solution was then read at 570 and 595 nm using a microplate reader (Spetrostarnano, BMG Labtech, UK).

Cell proliferation was assessed by quantifying the number of adherent cells to membranes with Quant-iT™ PicoGreen™ assay on days 2, 7, and 14. Briefly, cells were lysed and the supernatant solution was diluted in assay buffer followed by addition of Quant-iT™ PicoGreen™ reagent and incubation for 5 min at RT. Fluorescence of the samples was measured at 480 nm (excitation) and 520 nm (emission) using a microplate reader (Spetrostarnano, BMG Labtech, UK). The DNA concentration for each sample was calculated by using a standard curve.

DATA AVAILABILITY STATEMENT

The raw data supporting the conclusions of this article will be made available by the authors, without undue reservation.

AUTHOR CONTRIBUTIONS

AM, ES, AD, and AM designed the project, interpreted results, and wrote the article. CR-G, MG, KI-B, EC, and AR conducted experiments, analyzed data, etc.

ACKNOWLEDGMENTS

This work was supported by the ERC Starting Grant (STROFUNSCAFF), the Marie Curie Career Integration Grant (BIOMORPH), the AO Research Fund of the AO Foundation project number AOCMF-17-19M, and the UK Regenerative Medicine Platform (UKRMP2) Acellular Smart Materials. Also, the authors are grateful for funding from the Spanish Government (MAT2016-78903-R), Junta de Castilla y León (VA317P18), Interreg V A España Portugal POCTEP (0624_2IQBIONEURO_6_E), and Centro en Red de Medicina Regenerativa y Terapia Celular de Castilla y León. Furthermore, we would like to acknowledge the Program for Innovation and Human Capital from the Ministry of Science, Technology, and Telecommunications of the Republic of Costa Rica (MICITT-PINN-PED-014-2015-2).

REFERENCES

Azarniya, A., Eslahi, N., Mahmoudi, N., and Simchi, A. (2016). Effect of graphene oxide nanosheets on the physico-mechanical properties of chitosan/bacterial cellulose nanofibrous composites. *Compos. Part A Appl. Sci. Manuf.* 85, 113–122. doi: 10.1016/j.compositesa.2016.03.011

Azevedo, H. S. (2019). "Biomaterials inspired by biology: from molecules to self-assembly," *Reference Module in Biomedical Sciences*, 109–117.

Capito, R. M., Azevedo, H. S., Velichko, Y. S., Mata, A., and Stupp, S. I. (2008). Self-assembly of large and small molecules into hierarchically ordered sacs and membranes. *Science* 319, 1812–1816. doi: 10.1126/science.1154586

Depan, D., Pesacreta, T. C., and Misra, R. D. K. (2014). The synergistic effect of a hybrid graphene oxide-chitosan system and biomimetic mineralization on osteoblast functions. *Biomater. Sci.* 2, 264–274. doi: 10.1039/C3BM60192G

Dinescu, S., Ionita, M., Pandele, A. M., Galateanu, B., Iovu, H., Ardelean, A., et al. (2014). *In vitro* cytocompatibility evaluation of chitosan/graphene oxide 3D scaffold composites designed for bone tissue engineering. *Biomed. Mater. Eng.* 24, 2249–2256. doi: 10.3233/BME-141037

Discher, D. E., Janmey, P., and Wang, Y. L. (2005). Tissue cells feel and respond to the stiffness of their substrate. *Science* 310, 1139–1143. doi: 10.1126/science.1116995

Draper, E. R., Eden, E. G., McDonald, T. O., and Adams, D. J. (2015). Spatially resolved multicomponent gels. *Nat. Chem.* 7, 848–852. doi: 10.1038/nchem.2347

Gazit, E. (2007). Self-assembled peptide nanostructures: the design of molecular building blocks and their technological utilization. *Chem. Soc. Rev.* 36:1263. doi: 10.1039/b605536m

Gentile, P., Ferreira, A. M., Callaghan, J. T., Miller, C. A., Atkinson, J., Freeman, C., et al. (2017). Multilayer nanoscale encapsulation of biofunctional peptides to enhance bone tissue regeneration *in vivo*. *Adv. Healthc. Mater.* 6:1601182. doi: 10.1002/adhm.201601182

Han, D., Yan, L., Chen, W., and Li, W. (2011). Preparation of chitosan/graphene oxide composite film with enhanced mechanical strength in the wet state. *Carbohydr. Polym.* 83, 653–658. doi: 10.1016/j.carbpol.2010.08.038

Hedegaard, C. L., Collin, E. C., Redondo-Gómez, C., Nguyen, L. T., Ng, K. W., Castrejón-Pita, A. A., et al. (2018). Hydrodynamically guided hierarchical self-assembly of peptide-protein bioinks. *Adv. Funct. Mater.* 28:1703716. doi: 10.1002/adfm.201703716

Inostroza-Brito, K. E., Collin, E., Siton-Mendelson, O., Smith, K. H., Monge-Marcet, A., Ferreira, D. S., et al. (2015). Co-Assembly, spatiotemporal control and morphogenesis of a hybrid protein-peptide system. *Nat. Chem.* 7, 897–904. doi: 10.1038/nchem.2349

Inostroza-Brito, K. E., Collin, E. C., Majkowska, A., Elsharkawy, S., Rice, A., Armando, E., et al. (2017). Cross-linking of a biopolymer-peptide co-assembling system. *Acta Biomater.* 58, 80–89. doi: 10.1016/j.actbio.2017.05.043

Jalaja, K., Sreehari, V. S., Kumar, P. R. A., and Nirmala, R. J. (2016). Graphene oxide decorated electrospun gelatin nanofibers: fabrication, properties and applications. *Mater. Sci. Eng. C* 64, 11–19. doi: 10.1016/j.msec.2016.03.036

Justino, C. I. L., Gomes, A. R., Freitas, A. C., Duarte, A. C., and Rocha-Santos, T. A. P. (2017). Graphene based sensors and biosensors. *TrAC Trends Anal. Chem.* 91, 53–66. doi: 10.1016/j.trac.2017.04.003

Kang, S., Park, J. B., Lee, T. J., Ryu, S., Bhang, S. H., La, W. G., et al. (2015). Covalent conjugation of mechanically stiff graphene oxide flakes to three-dimensional collagen scaffolds for osteogenic differentiation of human mesenchymal stem cells. *Carbon* 83, 162–172. doi: 10.1016/j.carbon.2014.11.029

Kumar, M., Ing, N. L., Narang, V., Wijerathne, N. K., Hochbaum, A. I., and Ulijn, R. V. (2018). Amino-acid-encoded biocatalytic self-assembly enables the formation of transient conducting nanostructures. *Nat. Chem.* 10, 696–703. doi: 10.1038/s41557-018-0047-2

Lee, J. H., Lee, Y., Shin, Y. C., Kim, M. J., Park, J. H., Hong, S. W., et al. (2016). *In situ* forming gelatin/graphene oxide hydrogels for facilitated C2C12 myoblast differentiation. *Appl. Spectrosc. Rev.* 51, 527–539. doi: 10.1080/05704928.2016.1165686

Li, J., Ren, N., Qiu, J., Mou, X., and Liu, H. (2013). Graphene oxide-reinforced biodegradable genipin-cross-linked chitosan fluorescent biocomposite film and its cytocompatibility. *Int. J. Nanomed.* 8, 3415–3426. doi: 10.2147/IJN.S51203

Lin, J., Chen, X., and Huang, P. (2016). Graphene-based nanomaterials for bioimaging. *Adv. Drug Deliv. Rev.* 105, 242–254. doi: 10.1016/j.addr.2016.05.013

Liu, J., Cui, L., and Losic, D. (2013). Graphene and graphene oxide as new nanocarriers for drug delivery applications. *Acta Biomater.* 9, 9243–9257. doi: 10.1016/j.actbio.2013.08.016

Mata, A., Hsu, L., Capito, R., Aparicio, C., Henrikson, K., and Stupp, S. I. (2009). Micropatterning of bioactive self-assembling gels. *Soft Matter* 5, 1228–1236. doi: 10.1039/b819002j

Mata, A., Palmer, L., Tejeda-Montes, E., and Stupp, S. I. (2012). Design of biomolecules for nanoengineered biomaterials for regenerative medicine. *Methods Mol. Biol.* 811, 39–49. doi: 10.1007/978-1-61779-388-2_3

Mazaheri, M., Akhavan, O., and Simchi, A. (2014). Flexible bactericidal graphene oxide-chitosan layers for stem cell proliferation. *Appl. Surf. Sci.* 301, 456–462. doi: 10.1016/j.apsusc.2014.02.099

Mendes, A. C., Baran, E. T., Reis, R. L., and Azevedo, H. S. (2013). Self-assembly in nature: using the principles of nature to create complex nanobiomaterials. *Wiley Interdiscip. Rev. Nanomed. Nanobiotechnol.* 5, 582–612. doi: 10.1002/wnan.1238

Navon, Y., and Bitton, R. (2016). Elastin-like peptides (ELPs) building blocks for stimuli-responsive self-assembled materials. *Isr. J. Chem.* 56, 581–589. doi: 10.1002/ijch.201500016

Newcomb, C. J., Sur, S., Ortony, J. H., Lee, O. S., Matson, J. B., Boekhoven, J., et al. (2014). Cell death versus cell survival instructed by supramolecular cohesion of nanostructures. *Nat. Commun.* 5:3321. doi: 10.1038/ncomms4321

Okesola, B. O., Lau, H. K., Derkus, B., Boccorh, D. K., Wu, Y., Wark, A. W., et al. (2020a). Covalent co-assembly between resilin-like polypeptide and peptide amphiphile into hydrogels with controlled nanostructure and improved mechanical properties. *Biomater. Sci.* 8, 846–857. doi: 10.1039/C9BM01796H

Okesola, B. O., and Mata, A. (2018). Multicomponent self-assembly as a tool to harness new properties from peptides and proteins in material design. *Chem. Soc. Rev.* 47, 3721–3736. doi: 10.1039/C8CS00121A

Okesola, B. O., Ni, S., Derkus, B., Galeano, C. C., Hasan, A., Wu, Y., et al. (2020b). Growth-factor free multicomponent nanocomposite hydrogels that stimulate bone formation. *Adv. Funct. Mater.* 30:1906205. doi: 10.1002/adfm.201906205

Okesola, B. O., Wu, Y., Derkus, B., Gani, S., Wu, D., Knani, D., et al. (2019). Supramolecular self-assembly to control structural and biological properties of multicomponent hydrogels. *Chem. Mater.* 31, 7883–7897. doi: 10.1021/acs.chemmater.9b01882

Pashuck, E. T., Cui, H., and Stupp, S. I. (2010). Tuning supramolecular rigidity of peptide fibers through molecular structure. *J. Am. Chem. Soc.* 132, 6041–6046. doi: 10.1021/ja908560n

Perczel, A., and Fasman, G. D. (1992). Quantitative analysis of cyclic beta-turn models. *Protein Sci.* 26, 1527–1572.

Rajan Unnithan, A., Ramachandra Kurup Sasikala, A., Park, C. H., and Kim, C. S. (2017). A unique scaffold for bone tissue engineering: an osteogenic combination of graphene oxide–hyaluronic acid–chitosan with simvastatin. *J. Ind. Eng. Chem.* 46, 182–191. doi: 10.1016/j.jiec.2016.10.029

Raymond, D. M., and Nilsson, B. L. (2018). Multicomponent peptide assemblies. *Chem. Soc. Rev.* 47, 3659–3720. doi: 10.1039/C8CS00115D

Redondo-Gómez, C., Abdouni, Y., Becer, C. R., and Mata, A. (2019). Self-assembling hydrogels based on a complementary host-guest peptide amphiphile pair. *Biomacromolecules* 20, 2276–2285. doi: 10.1021/acs.biomac.9b00224

Schneider, C. A., Rasband, W. S., and Eliceiri, K. W. (2012). NIH image to imageJ: 25 years of image analysis. *Nat. Methods* 9, 671–675. doi: 10.1038/nmeth.2089

Shao, L., Chang, X., Zhang, Y., Huang, Y., Yao, Y., and Guo, Z. (2013). Graphene oxide cross-linked chitosan nanocomposite membrane. *Appl. Surf. Sci.* 280, 989–992. doi: 10.1016/j.apsusc.2013.04.112

Shin, S. R., Li, Y. C., Jang, H. L., Khoshakhlagh, P., Akbari, M., Nasajpour, A., et al. (2016). Graphene-based materials for tissue engineering. *Adv. Drug Deliv. Rev.* 105, 255–274. doi: 10.1016/j.addr.2016.03.007

Stankovich, S., Piner, R. D., Nguyen, S. B. T., and Ruoff, R. S. (2006). Synthesis and exfoliation of isocyanate-treated graphene oxide nanoplatelets. *Carbon* 44, 3342–3347. doi: 10.1016/j.carbon.2006.06.004

Stephanopoulos, N., Ortony, J. H., and Stupp, S. I. (2013). Self-assembly for the synthesis of functional biomaterials. *Acta Mater.* 61, 912–930. doi: 10.1016/j.actamat.2012.10.046

Tang, H., Liu, D., Zhao, Y., Yang, X., Lu, J., and Cui, F. (2015). Molecular dynamics study of the aggregation process of graphene oxide in water. *J. Phys. Chem. C* 119, 26712–26718. doi: 10.1021/acs.jpcc.5b07345

Wan, C., Frydrych, M., and Chen, B. (2011). Strong and bioactive gelatin-graphene oxide nanocomposites. *Soft Matter* 7, 6159–6166. doi: 10.1039/c1sm05321c

Webber, M. J., Tongers, J., Renault, M. A., Roncalli, J. G., Losordo, D. W., and Stupp, S. I. (2010). Development of bioactive peptide amphiphiles for therapeutic cell delivery. *Acta Biomater.* 6, 3–11. doi: 10.1016/j.actbio.2009.07.031

Whitesides, G. M., and Grzybowski, B. (2002). Self-assembly at all scales. *Science* 295, 2418–2421. doi: 10.1126/science.1070821

Wick, P., Louw-Gaume, A. E., Kucki, M., Krug, H. F., Kostarelos, K., Fadeel, B., et al. (2014). Classification framework for graphene-based materials. *Angew. Chem. Int. Ed.* 53, 7714–7718. doi: 10.1002/anie.201403335

Yang, Y., Asiri, A. M., Tang, Z., Du, D., and Lin, Y. (2013). Graphene based materials for biomedical applications. *Mater. Today* 16, 365–373. doi: 10.1016/j.mattod.2013.09.004

Zhang, S. (2003). Fabrication of novel biomaterials through molecular self-assembly. *Nat. Biotechnol.* 21, 1171–1178. doi: 10.1038/nbt874

Zhang, S., Greenfield, M. A., Mata, A., Palmer, L. C., Bitton, R., Mantei, J. R., et al. (2010). A self-assembly pathway to aligned monodomain gels. *Nat. Mater.* 9, 594–601. doi: 10.1038/nmat2778

Zhou, X., Nowicki, M., Cui, H., Zhu, W., Fang, X., Miao, S., et al. (2017). 3D bioprinted graphene oxide-incorporated matrix for promoting chondrogenic differentiation of human bone marrow mesenchymal stem cells. *Carbon* 116, 615–624. doi: 10.1016/j.carbon.2017.02.049

Zhu, Y., Murali, S., Cai, W., Li, X., Suk, J. W., Potts, J. R., et al. (2010). Graphene and graphene oxide: synthesis, properties, and applications. *Adv. Mater.* 22, 3906–3924. doi: 10.1002/adma.201001068

Conflict of Interest: The authors declare that the research was conducted in the absence of any commercial or financial relationships that could be construed as a potential conflict of interest.